International Journal of Communication Networks and Information Security

ISSN: 2073-607X, 2076-0930

*Volume **14** Issue **02 Year 2022** Page **83:98***

Adaptive And Reliable GPS Uncertain Position Estimation an Insightful Oceanography and Geography Applications

K Uday Kiran[1], S. Koteswara Rao[2], K.S. Ramesh[3]

[1]Assistant Professor, Dept. of ECE, KL University, Guntur, A.P, India

[2, 3] Professor, Dept. of ECE, KL University, Guntur, A.P, India

uk_ece@kluniversity.in, skrao@kluniversity.in, dr.ramesh@kluniversity.in

Article History

Received: 22 Feb 2022
Revised: 18 May 2022
Accepted: 17 June 2022

Abstract

Location evaluation applications are one of the most imperative services in GPS position applications. The Global Positioning Systems (GPS) is a versatile and legacy technology has been providing a reliable and accurate position of objects on Earth. The uncertain GPS position is considered an initialization parameter for many inherent systems in today's world. This initialization position estimate has a wide variety of applications such as Coast line maps, understanding the geo-dynamical phenomena such as volcanic eruptions, earthquakes and subsequent originating source mechanisms, Mean Sea level estimation for contours of land surfaces, Oceanic en-route as well as in mobile and Vehicular technologies etc. The validation and reliability of the results of all those applications is dependent on the accuracy of the position estimate given by GPS. In this work an attempt is made to retrieve accurate and reliable position parameters from GPS by correcting the measurement errors for all the visible satellites at every epoch. The maximum and minimum pseudo ranges in L2 signal observed are 2437404.2 meters and -76295.22 meters.

Keywords: Statistical signal processing, uncertain GPS, geography, receiver-estimation

1. Introduction

GPS is a-well-established tool for both scientific research and technological studies. Precise GPS position estimation has a wide range of applications in today's world. Some of the decisive applications are outlined here. Coast line surveys are conducted to identify the land and sea or ocean border, where the position estimation has long-term, cyclic, and random variations [1]. These variations may depend on specific events such as earthquakes, Tsunamis etc. In such studies the mapping of the coast line depends on the spatiotemporal scales and the instruments used to measure them. Earthquake and volcanic, detection and prediction are emerging research areas where the geo-dynamical phenomena and their source mechanisms have a larger impact on the tectonic plate movement [2]. GPS devices are also used to mark the contours between local ground motion and sea level where the variations are dependent on the spatiotemporal scales of the electronic position estimators [3]. One of the most crucial applications is

oceanic en-route, where the position estimation is relative and its accuracy depends on the spatiotemporal effects of the instruments and the physical systems. These signals are influenced by the space weather systems such as Ionosphere and Atmosphere through which they are traversing.

There are many scientific studies and applications wherein, the GPS is used as a versatile tool in various technological advancements such as mobile and vehicular navigation systems. In all these applications the position estimates are relative and are dependent on the spatiotemporal errors in GPS [4].

Relative positioning is conceptualized as computation of the position vector between two or more GPS receivers or a temporal routine in a single platform. The temporal behavior of the errors is of utmost importance in position estimation using GPS. The study of the relative variability of the errors leads us to postulate certain algorithms and approaches for precise and post-mission satellite information [5].

Nowadays there are many satellite-based navigations systems that cater navigation information to the world. The Global Navigation Satellite System (GNSS) provides time, as a crucial fourth dimension. The positional accuracy of GNSS mainly depends on the precise measurement of time stamp of the signal and also on its traversing time from the source to destination [6]. The GPS or the GNSS satellites encompass atomic clocks, which contribute to very precise time data to the GPS or the GNSS signals. The receivers decode these signals and synchronize with the atomic clocks and thereby determine accurate time within 100*10^6 of a second, without owning an atomic clock [7]. Thus, the accuracy in time information provides precise positioning of the satellite in its orbit. Hence, the pseudo-ranges thus measured from the receiver makes them precise [8].

From this, it is well understood that the satellite and receiver clock errors need to be corrected so as to obtain a precise positioning of GPS or GNSS systems. Owing to the computational issues or the availability of the GPS data, pseudo-ranges for all the visible satellites are directly taken from the RINEX observation file [9]. Till date at any certain epoch of time of study have 8-12 visible satellites at any point on earth. The pseudo-ranges obtained at that epoch will not match with each other as the satellites are in different places in their respective orbits. It is therefore, the batch processing of the pseudo-ranges irrespective of the satellite orbital position for a sampled time of 30sec provides the degree of inaccuracy in estimating the GPS receiver precise positioning [10]. The pseudo-ranges measured by the GPS receivers are not accurate as the signals are affected by the temporal errors due to satellite and receiver clocks, orbital errors, ionosphere, and atmosphere [11][12].

GPS signal must be processed to reduce these errors so as to compute precise positioning. The GPS receivers are calibrated using kinematic processing for several minutes to acquire precise positioning to extract initialization parameters. Kinematic relative positioning is also having measurement errors [13]. Conventional GPS calibration methods -batch processing and kinematic processing of GPS the carrier phase ambiguities are fixed at their first occurrence. These are not changed and corrected for other incidents of their occurrence [14]. Epoch processing of GPS data results in a trade-off between the computation time and accurate positioning when compared with the conventional processing techniques [15].

In the present work satellite clock offset, receiver clock offset, orbital or ephemeris errors are corrected for all the visible satellites for every epoch. The resulted pseudo-ranges and the other parameters are averaged at every epoch so compute precise positioning [16]. The results will be will be more precise if the methodology is implemented for both L1 and L2 signals.

2. Literature Survey

In this section, facilitates brief discussions on various GPS Position Estimation systems & their performance. The following survey has not tolerant some issues like Coast line maps, understanding the geo-dynamical phenomena such as volcanic eruptions, earthquakes and subsequent originating source mechanisms, Mean Sea level estimation for contours of land surfaces, Oceanic en-route as well as in

mobile and Vehicular technologies etc. Hence, an advanced Adaptive and Reliable GPS uncertain Position Estimation system has been performed, which outperforms the past models with accurate and reliable position parameters.

Coastal risk and adaptation assessments must better anticipate the publication of fresh and updated sea-level rise (SLR) information by Nicholls, R. J [2021], such as that from the IPCC Assessment Reports. Since new information constantly emerges, it is imperative that previous estimates of risk and adaptability be revisited and revised as appropriate. For sea-level extremes, revised advise is provided in this publication. If the headline forecasted ranges in all IPCC reports are compared, the most recent "Special Report on Ocean and Cryosphere in Changing Climate" shows a rise since the fourth and fifth assessments. The Greenland/Antarctic ice sheet components are a major source of uncertainty, and IPCC reports have started to incorporate this in their analyses, emphasising the relevance of possible high-end sea-level responses. The approaches proposed here are practical and take coastal risk assessment, adaptation planning, and long-term decision-making into account as a continual process and guarantee that pragmatic adaptation choices may be made despite huge uncertainties. Recent findings on sea level rise are not automatically a reason to throw out previous assessments, but rather an opportunity to reexamine both the robustness of previous assessments considering new science and the usefulness of proactive adaptation and planning strategies, especially considering longer-term uncertainties.[1]

Allison, L. C [2022] Since the end of the 19th century, global mean sea level has risen because of global warming. Rising sea levels are expected to continue for the rest of this century and into the next. In addition to the global mean signal, the amount of sea level rise varies greatly among regions. For coastal management planning, accurate forecasts of future sea level rise are essential at the local level. This study used tide gauge records and satellite altimetry data to conduct an observational study of recent sea level fluctuations along the South African coast. This pace of sea level rise surrounding South Africa has been consistent with projections of global mean sea level rise over the last several decades, according to this study. Eight locations along the South African coast were chosen for sea level projections under low emissions scenarios (RCP2.6) and high emissions scenarios (RCP8.5). Existing methods (rooted in the methods of the Fifth Assessment Report of the Intergovernmental Panel on Climate Change, but with several methodological innovations) were used.[2]

Kint, L [2021] obviously, a data selection technique that is designed to increase the reliability of data products lowers the amount of data available. To what extent this change in density impacts data products' geographical coverage will be determined by their intended application. If there are noticeable gaps in geographical coverage, they might serve as a reminder of the need for further data collection and better survey design. In order to provide policymakers and other end users with a clearer picture of the overall level of confidence in the subsurface model and the accompanying data uncertainties, this research have integrated the proposed model into a decision support tool that is available to the general public. As the depth of the borehole dataset decreases, engineering geologists and geospatial analysts will benefit most from a more accurate depiction of the uncertainty that comes along with that depth.[3]

McCammon, S [2021] Ocean monitoring is costly and time-consuming, but autonomous robots can help. In this study, demonstrate a system for autonomously identifying and monitoring ocean fronts using a team of ASVs and UUVs (AUVs). The main contributions of this study are (1) proposed algorithm for autonomous coordination using general autonomy principles: Sequential Allocation Monte Carlo Tree Search (SA-MCTS), which incorporates domain knowledge into environmental estimation by augmenting a standard Gaussian process with a nearest neighbours prior and planning in a drifting reference frame, and (2) decision support user interface to help human operators oversee the autonomous system. This study wants to bridge the gap between cutting-edge autonomous algorithms and field-tested maritime vehicle planning methodologies. This study introduces a broad, heuristic-based multi-robot coordination technique for extended sampling.[4]

Borrelli, M [2021] Coastal regions are challenging to scan with high-resolution acoustic vessels. In shallow (20 m) coastal waters, phase-measuring side scan sonar is becoming increasingly popular. The principal author discusses field instruments from the past decade. This is an introduction to the operation, usage, and data sets of these equipment for coastal scientists. Hydrographers unfamiliar with phase-

measuring side scan sonar will learn about survey design, data collecting, and processing. Co-located sides can backscatter and swath bathymetry are collected. Phase-measuring sides can sonars are useful for shallow water imaging due to their wider bathymetric swaths. Large effective swath widths reduce noise and processing in bathymetric data sets compared to multibeam data. The side scan backscatter and bathymetric data sets can be utilized independently, but co-location enables new applications and analysis. These tools are useful for seabed mapping and scientific research. The data and ideas offered here may assist the shallow water mapping community and multi-disciplinary organizations.[5]

3. Data Considered

In this section, the GPS data considered for analysis is collected from the Novatel GPS receiver installed at India Meteorological Department (IMD), Machilipatnam.

GPS Receiver station at IMD, Machilipatnam (16° 12′ N, 81° 08′ E),
Dual Frequency GPS Receiver and Antenna
(Model: GPS Station6 Make: Atel), Installed on 20th September 2014 Sanctioned under DST Project,
File No: SR/S4/AS-91/20121

Figure: 1 represents the GPS Receiver installed at IMD Machilipatnam

Station Number	Station Name	Geo. Lat. (°N)	Geo. Long. (°E)	Geom. Lat. (°N)	Geom. Long. (°E)
1	Jodhpur (JOD)	26.26	73.05	17.75	147.16
2	Delhi (DL)	28.58	77.21	19.68	151.29
3	Bangalore (BAN)	12.95	77.68	4.08	150.24
4	Hyderabad (HYD)	17.45	78.47	8.49	151.41
5	Bhopal (BPL)	23.29	77.62	14.38	151.14
6	Lucknow (LKW)	26.76	80.88	17.57	154.53
7	Simla (SIM)	31.08	77.066	22.18	151.42
8	Agatti (AGT)	10.83	72.17	2.49	144.65
9	Trivandrum (TRM)	8.48	76.92	−0.31	149.08
10	Bagdodra (BAG)	26.68	88.32	16.99	161.46
11	Aizwal (AIZ)	23.84	92.62	13.94	165.32
12	Guwahati (GHT)	26.12	91.59	16.26	164.48
13	Kolkatta (KOL)	22.18	88.44	12.49	161.28
14	Raipur (RAI)	21.18	81.74	11.94	154.86
15	Vizog (VIZ)	17.75	83.22	8.41	155.99
16	Mumbai (MUM)	19.09	72.85	10.64	146.18
17	Ahmedabad (AHMD)	23.064	72.62	14.61	146.40
18	Portblair (PTBR)	11.67	92.725	1.78	164.83

Figure: 2 Represents the Image list of GPS Receiver Locations Installed in India

The data is collected on 17 March 2017 a geomagnetic storm day. Fig.1 represents GPS receiver & fig 2

represents some of the GPS Receiver Locations Installed in India [18-21].

4. Methodology

In this section, the GPS calculates the position by calculating the distance between the ground-based receiver, the GPS satellite and calculation of position of the uncertain GPS satellite in its orbit. To calculate the satellite position in the orbit the GPS time is used to calculate mean motion of the satellite. So, the time correction of the satellite and the receiver is most important for finding the accurate position of the satellite in its orbit. [22]

The distance between the satellite and the receiver is calculated by considering the time stamp in the signal transmitted by the GPS satellite. The GPS deals with three-time scales. They are time kept by the satellite clock (ts), the time kept by the receiver clock (tr) and the common reference time the GPST (tGPST). The GPS time tGPST is defined in terms of seconds of week or week number or number of seconds of week. The satellite clock bias is relative to tGPST and is modelled and uploaded by the master control station. These parameters are broadcasted as part of the navigation message [23-25].

At a given epoch of time the signals the transmitted time from all the visible satellites is same [26]. The only difference between the signals is the clock error in each satellite [27]. The absolute transmit time is calculated by the using the pseudo-ranges on L2 GPS signal, given in the RINEEX GPS data. The absolute transmit time is show in below eq (1)

$$t\_p_2 = \rho_{L2} / C \qquad (1)$$

where ρ_{L_2} is the pseudo-ranges on L2 and C is the velocity of light. So the time at which the signal is received by the GPS receive is given as show in below eq (2)

$$t_{rx} = t_{rx-raw} + t\_p_2 \qquad (2)$$

where trx is the time at which the signal is received. So the receiver clock offset is given by eq (3)

$$t_{rx-raw} = t_{rx} - t\_p_2 \qquad (3)$$

The pseudo-ranges of every satellite are different as they are in different positions in their respective orbits. The receiver times are also different for all the satellites at the considered epoch [28]. An optimized receiving time has to be considered so as to compute the precise satellite position in the orbit and from which the pseudo-ranges are calculated. The pseudo-ranges which is available in the RINEX data is the measured pseudo-ranges. The time of signal transition and is called as time of epoch toe given is the navigation data. The time of epoch toe is same and the transmission and reception times are different for all the visible satellites at that instant [29, 30].

The epoch time which effects on the accuracy of the pseudo-ranges which has to be corrected. The GPS system time which is given as GPS Time of week (TOW) or tGPST is used considered for the further analysis. The difference between tGPST and toe must be accounted for the beginning and end of the week crossovers. It is implemented as follows. [Fundamentals of GPS]

$$If\ t_k = tGPST - toe > 302400\ then\ t_k = t_k - 604800$$

and

$$If\ t_k = tGPST - toe > 302400\ then\ t_k = t_k + 604800$$

Or else

$$t_k = t_k \qquad (4)$$

The correction of the clock errors is implemented as follows. The time correction obtained by the above equation is called δt1 and is obtained by replacing the toe by t_p2 for that satellite. The corrected time δt1

is called the first correction tcorr1. The first-time correction tcorr1 is then corrected for the satellite clock offset, fractional frequency offset (seconds/sec), and the fractional frequency drift (seconds/sec2) given by $a_{f_0}, a_{f_1}, a_{f_2}$ respectively as given below equation (5) and (6).

The fist corrected GPST is given as

$$t_{rx-GPSTI} = t_{rx-raw} - t_{corr1} \quad (5)$$

$$t_{corr1} = a_{f2} * \delta t_1 + a_{f1} * \delta t_1 + a_{f0} * \delta t_1 \quad (6)$$

The trx_raw is calculated from the year, month, date, hours and seconds data given in the first observations of the Observation file (.Obs) in the RINEX format. Now the time is corrected for the satellite clock offset by subtitling the tx_GPST in Eq.4. The corrected time then is called as the second time correction δt2. The second time correction is corrected for the satellite clock errors as show in below eq (7)

$$t_{corr2} = a_{f1} * \delta t_2 + a_{f1} * \delta t_2 + a_{f0} * \delta t_2 \quad (7)$$

Then the corrected GPST is obtained by eq (8)

$$t_{x-GPST2} = t_{x-GPSTI} - t_{corr2} - t_{GD} \quad (8)$$

where tGD group time delay of the signal after traversing from the ionosphere. This tx_GPST2 will be corrected GPST for that epoch for a particular satellite denoted as tk the instantaneous time. Now after correcting the time for both the satellite and receive clock errors for the instantaneous time the satellite position is calculated as follows.

$$n_1 = \sqrt{\frac{\mu}{a_1^3}} + \Delta n \quad (9)$$

The mean motion if the satellite is given as where μ=3.986005*10^14 m3/sec2 called as the earth's universal Gravitational Constant and a1 is the square of the semi-major axis of the satellite orbit and Δn is the mean motion difference from the computed value given in rads-1. From eq (9) mean anomaly is computed as show in below eq (10)

$$M_1 = M_0 + n_1(t_k) \quad (10)$$

where M0 is the mean anomaly at reference time toe. The eccentricity of the satellite orbit is computed as follows eq (11).

$$ecc = M_1 + e_s \, sin(ecc) \quad (11)$$

Where *ecc* is the eccentric anomaly and es is the eccentricity of the orbit. The above equation is solved by using Newton-Raphson 's method. Let now the relativistic correction is given as show in below eq (12) and (13)

$$F1 = \frac{-2\sqrt{\mu}}{C^2} = -4.44280^{*}10^{\wedge} - \frac{10sec}{\sqrt{meter}} \quad (12)$$

$$\Delta tr = Fe_s\sqrt{a_{1s}}sin(ecc) \quad (13)$$

The relativistic correction is subtracted from the corrected instantaneous time tk and the final corrected time is called the tk1 which us used in computation of satellite position. This is given as show in below eq (14)

$$t_{k1} = t_k - \Delta tr \quad (14)$$

Now the true anomaly is calculated as show in below eq (15) and (16)

$$sin(v_k) = \frac{\sqrt{1 - e_s^2}\big(sin(ecc)\big)}{1 - e_s^2 \, cos(ecc)} \quad (15)$$

$$Cos(v_k) = \frac{cos(ecc) - e_s}{1 - e_s\, cos(ecc)} \quad (16)$$

The argument of latitude and its correction are given by eq (17)

$$\varphi_{k1} = v_{k1} + \omega \quad (17)$$

Corrected argument of latitude is given by eq (18)

$$\delta\varphi_{k1} = c_{us1}\, sin(2\varphi_{k1}) + c_{us1}\, cos(2\varphi_{k1}) \quad (18)$$

Where Cus1 and Cuc1 are the amplitude of sine and cosine correction to the argument of latitude which are given in RINEX navigation file

The radius of the satellite orbit is corrected as show in eq (19)

$$\delta r_{k1} = c_{rs1}\, sin(2\varphi_{k1}) + c_{rs1}\, cos(2\varphi_{k1}) \quad (19)$$

Where Crs1 and Crc1 are the amplitude of sine and cosine correction to orbital radius which are given in the RINEX data

The correction of orbital inclination is computed as show in below eq (20)

$$\delta i_{k1} = c_{is1}\, sin(2\varphi_{k1}) + c_{is1}\, cos(2\varphi_{k1}) \quad (20)$$

Where Cis1 and Cic1 are amplitude is the sine and cosine correction to the orbital inclination which are given in the RINEX data.

So, the corrected argument of latitude, corrected radius and inclination are given as show in below eq (21, 22, 23 and 24)

$$u_{k1} = \varphi_{k1} + \delta\varphi_{k1} \quad (21)$$

$$r_{k1} = a\big(1 - eco\, s(ecc)\big) + \delta r_{k1} \quad (22)$$

$$r_{k1} = a\big(1 - eco\, s(ecc)\big) + \delta r_{k1} \quad (23)$$

$$i_{k1} = i_0 + \left(di/_{dt}\right)t_{k1} + \delta r_{k1} \quad (24)$$

Where di/dt is the rate of change of inclination angle

The longitude node correction is calculated as

$$\Omega_{k1} = \Omega_0 + (\Omega - \Omega_e)t_{k1} - \Omega_e t_{0e} \quad (25)$$

Where Ωo is the longitude is ascending node of orbit plane at weekly epoch given in navigation data, $\dot{\Omega}$ is the rate of change of longitude of the ascending node and $\dot{\Omega}_e$ =7.2921151467*10^-05 rad/sec is the WGS-84 value of earth's rotation. Then the in-plane x and y position of the satellite are computed by below eq (26) & (27)

$$X_{p1} = r_{k1}\, cos(u_{k1}) \quad (26)$$

$$y_{p1} = r_{k1}\, sin(u_{k1}) \quad (27)$$

The satellite ECEF coordinates are computed as show in below eq (28), (29) and (30)

$$X_s = X_{p1}\, cos(\Omega_{k1}) - y_{p1}\, cos(i_{k1})\, sin(\Omega_{k1}) \quad (28)$$

$$y_s = X_{p1}\, sin(\Omega_{k1}) - y_{p1}\, cos(i_{k1})\, cos(\Omega_{k1}) \quad (29)$$

$$z_s = y_{p1}\, sin(i_{k1}) \quad (30)$$

The satellite ECEF coordinate frame is converted to local co-ordinate system i.e., East North up or ENU coordinate system by using coordinate conversion. Now the elevation angle and azimuth angle are computed as show in below eq (31) and (32)

$$E_{K1} = \arctan\left(\frac{x_{u1}}{\sqrt{x_N^2 + x_E^2}}\right) \quad (31)$$

$$A_{K1} = \arctan\left(\frac{x_E}{\sqrt{x_N}}\right) \quad (32)$$

where xE, xN and xU are the computed ENU coordinates. From the elevation angle and azimuth, the geographical and geomagnetic coordinate's i.e., the latitude and longitude of the GPS receiver are computed [19].

The above methodology is carried out on the RINEX data on 17th March 2017. The corrected plots for satellite position, pseudo range and radius of the orbit, inclination of the orbit and the ECEF and ENU coordinates are plotted for 0 to 30 sec for ease.

5. Results and Discussions

In this section proposed GPS system performance has been discussed from the above methodology, it is understood that correction in time leads to accurate estimation of satellite position in the orbit. The following are the steps undergone for consolidation of the results.

Step 1: Time correction is applied for all the visible satellites at a given epoch. In the present work the RINEX data from 10:0:0 to 10:0:30 UTC is considered for analysis.

Step 2: The corrected time tk is considered to compute the satellite position in the orbit.

Step 3: From the computed satellite positions, and the by

Using the receiver's ECEF coordinates given in the RINEX observation data pseudo-ranges are computed for all the visible satellites for every epoch.

Step 4: Along with the pseudo-ranges the corrected and uncorrected parameters are the GPS time, radius of the satellite's orbit, ECEF coordinates of the satellite, ENU coordinates of the satellite, elevation, and azimuth angles of the satellite in radians, latitude and longitude Ionospheric pierce point in degrees, total electron content (TEC) and some other parameters are also computed.

Step 5: The obtained values for all the visible satellites for at every epoch are averaged. For ease of representation only 30 second's data is plotted. All the parameters are for a one epoch are also plotted.

Fig.3 represents the averaged corrected GPS time (GPST in sec) for all the visible satellites for every epoch. It is observed that the time correction increases as the time of observation increases.

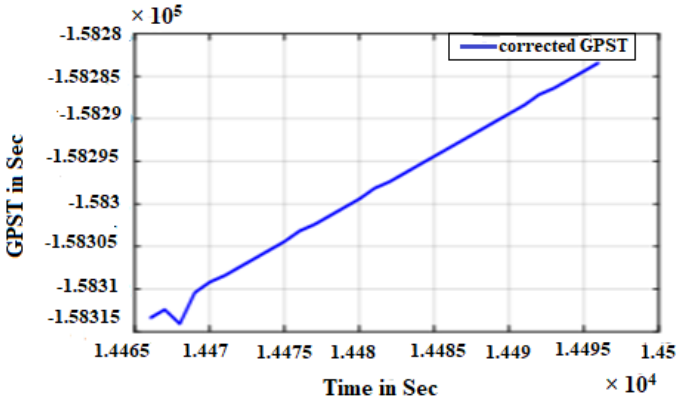

Figure: 3 Averaged corrected GPS Time in seconds.

The averaged uncorrected GPS time for all the visible satellites at every epoch is represented in the Fig.4. The difference in the averaged corrected and uncorrected GPS time for all the visible satellites at every epoch is shown in Fig.5.

Form the above figures it is understood that there is variation in the averaged corrected and uncorrected time is not constant. Thus, using the corrected GPST for all the visible satellites at every epoch, the radius of the satellite orbit, argument of latitude and corrected longitude of node are computed. The averaged corrected and uncorrected orbital radius for all the visible satellite at each epoch are represented in Fig.6 and in Fig.7 represents the averaged corrected and uncorrected argument of latitude. Fig.8 represents the averaged corrected and uncorrected longitude of node.

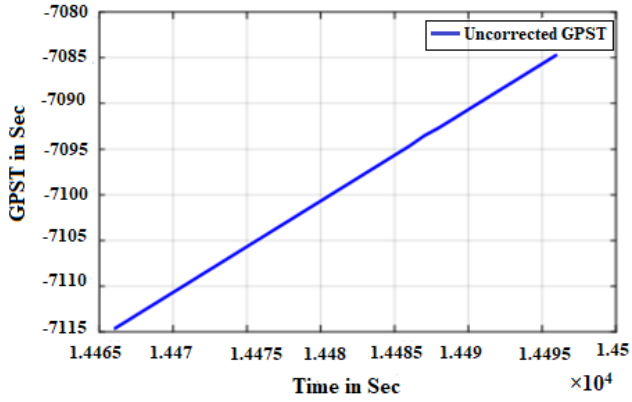

Figure: 4 Averaged uncorrected GPS time in seconds.

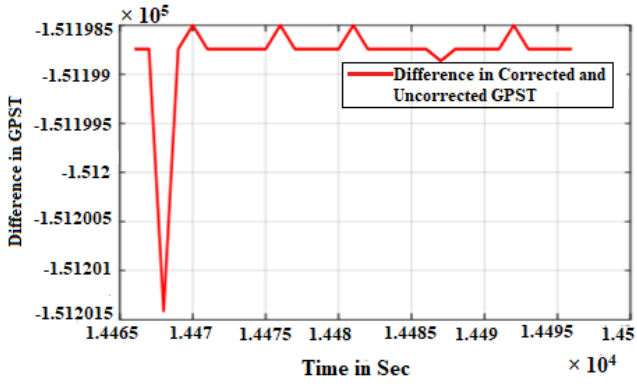

Figure: 5 Averaged differences in corrected and uncorrected GPS time in seconds.

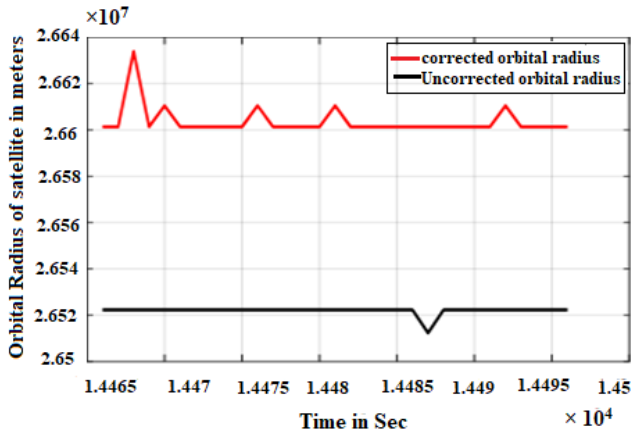

Figure: 6 Averaged corrected and uncorrected orbital radius in meters.

The averaged corrected ECEF satellite coordinates for all the visible satellites for every epoch are represented in the Fig.9 the averaged uncorrected ECEF satellite coordinates for all the visible satellites for every epoch are represented in Fig.10.

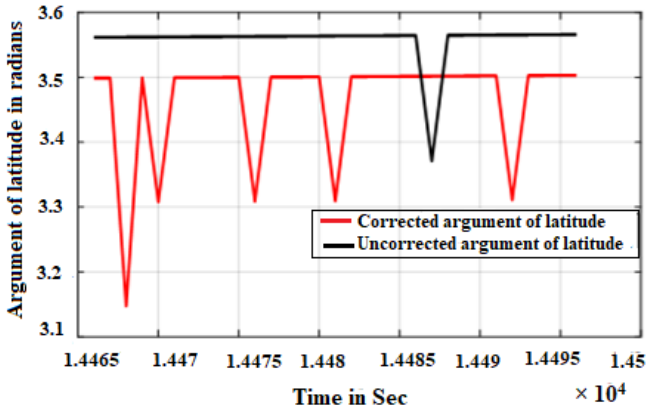

Figure: 7 Averaged corrected and uncorrected argument of latitude.

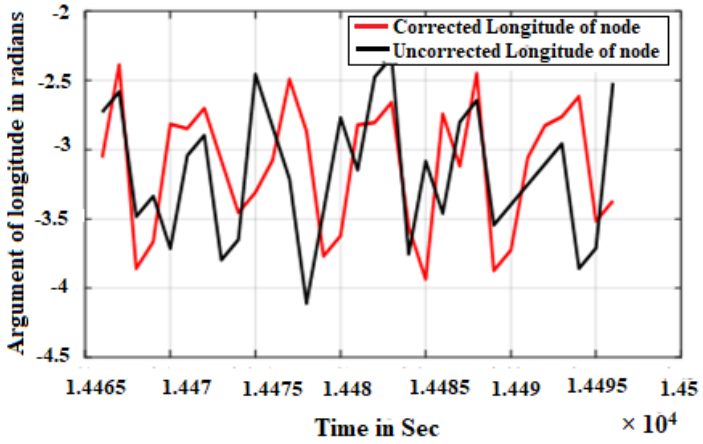

Figure: 8 Averaged corrected and uncorrected longitude of node.

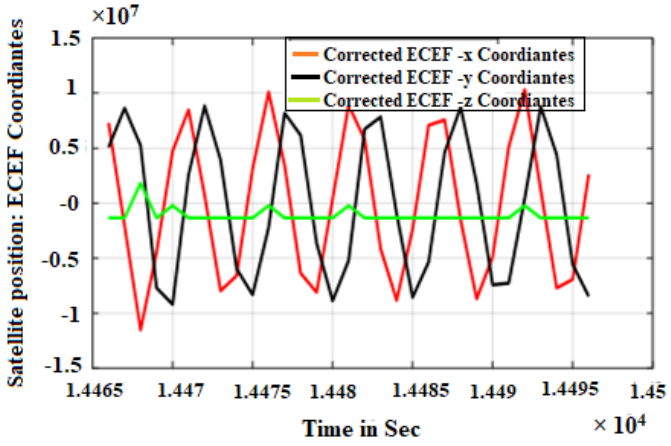

Figure: 9 Averaged corrected ECEF satellite coordinates.

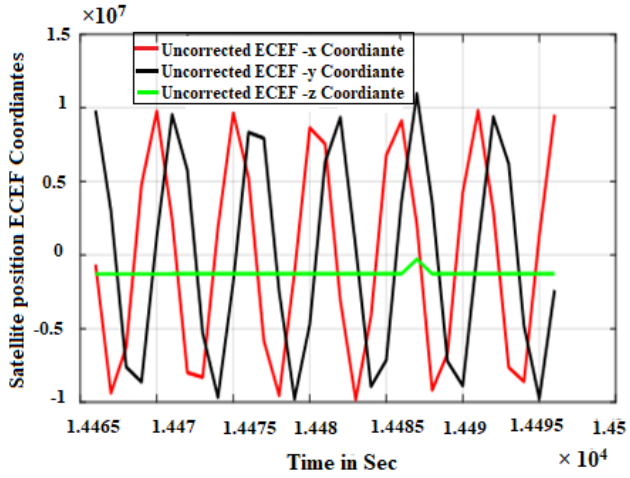

Figure: 10 Averaged uncorrected ECEF satellite coordinates.

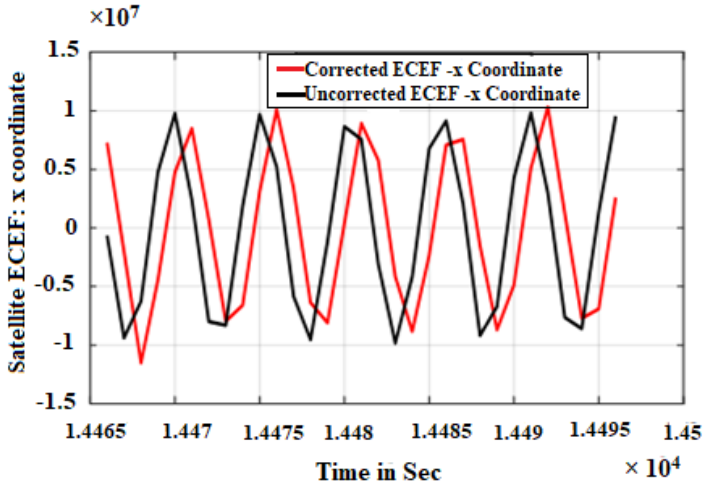

Figure: 11 Averaged corrected and uncorrected ECEF x coordinate.

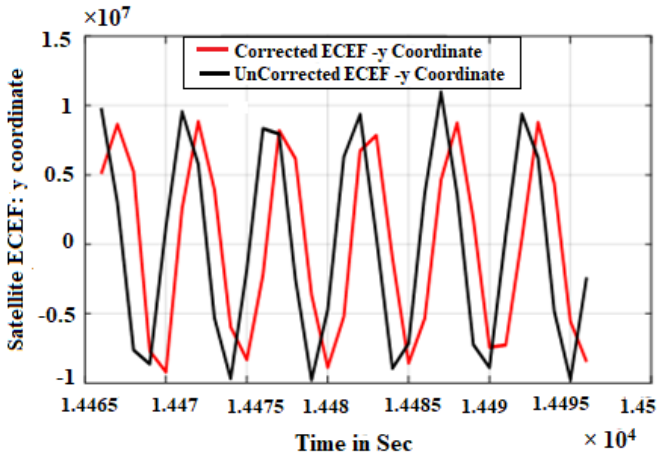

Figure: 12 Averaged corrected and uncorrected ECEF y coordinate.

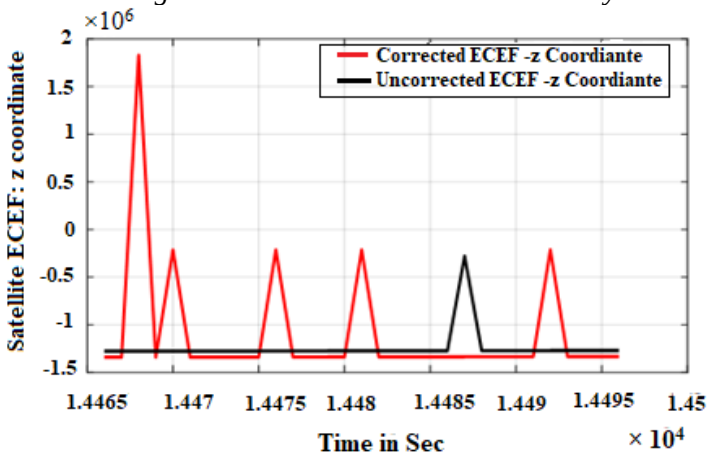

Figure: 13 Averaged corrected and uncorrected ECEF z coordinate.

The difference in the averaged corrected and uncorrected satellite ECEF coordinates separately are shown below. Fig.11 represents the ECEF x coordinate, Fig.12 represents the ECEF y coordinates, Fig.13 represents the ECEF z coordinates. The averaged corrected and uncorrected pseudo-ranges computed for all the visible satellites at every epoch are represented in the Fig.14.

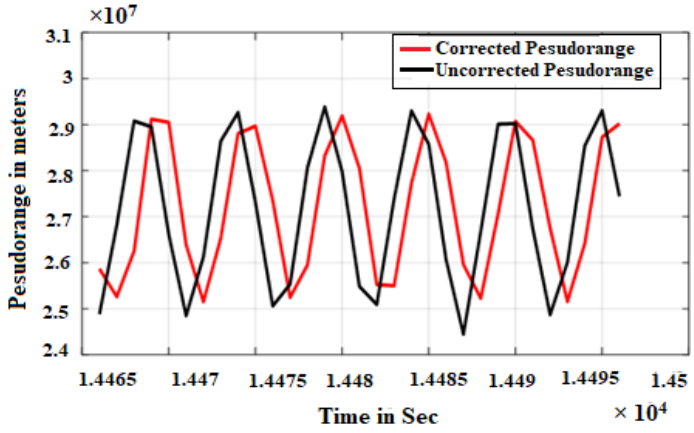

Figure: 14 Averaged corrected and uncorrected pseudo-ranges.

The averaged corrected and uncorrected elevation angle for all the visible satellite at every epoch is represented in the Fig.15. Similarly, the averaged corrected and uncorrected azimuth angles are

represented in the Fig.16. Now the latitude and longitude of ionosphere pierce points of the receiver position is in degrees.

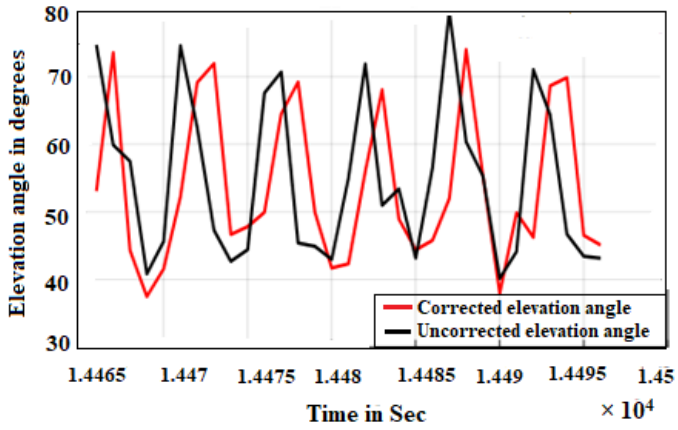

Figure: 15 Averaged corrected and uncorrected elevation angles.

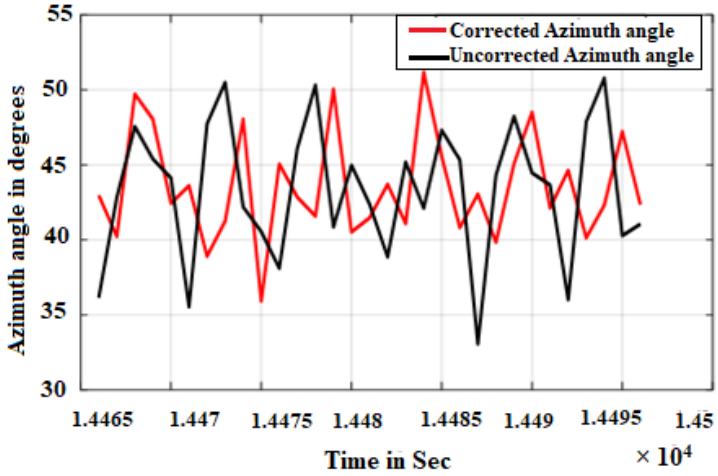

Figure: 16 Averaged corrected and uncorrected azimuth angles.

From the above results it is observed that the time correction for every visible satellite of each epoch has led to more optimum satellite position in orbit. Thus, it is able compute more accurate pseudo-ranges and receiver position compared to batch processing techniques and in the techniques where the statistical signal processing algorithms such as Kalman filter are applied directly on the pseudo-ranges obtained from the RINEX observation file. It also observed that averaging of the values of pseudo-ranges or receiver position to reduce the computation time does not provide a wise solution to the precise position estimation using GPS. The averaged difference between the corrected pseudo-ranges for 10 seconds is given in Table.1 given below.

Table: 1 Averaged corrected and uncorrected pseudo-ranges.

Sr .No	Corrected Pseudo-ranges in meters	Uncorrected Pseudo-ranges in meters	Difference in meters
1	25867222.55	24883832	983390.15
2	25261746.34	26811873	-550126.5

3	26252910.33	29077483	-824572.5
4	29117428.01	28951133	166295.11
5	29049003.61	26611599	2437404.2
6	26394116.79	24849050	1545066.9
7	25152059.9	26128355	-76295.22
8	26532444.77	28641131	-108686.4
9	28803907.54	29265493	-61585.81
10	28967341.52	27310714	1656627.1

From the table 1 below it is clearly seen that proposed system has both negative and positive values. In the batch processing technique these values are averaged at sampling time of 30 seconds where each second or epoch 8 to 12 visible satellites have. So approximately average is performed for between ranges of 240 values to 360 values irrespective of the satellite or PRN numbers assuming that all the above values are looking at a same position on earth.

6. Conclusion

The correction made in time, both satellite and receiver lead to compute a more accurate receiver position estimate from RINEX data files. From the findings, it can be shown that time correction for every observable satellite of each epoch has improved satellite orbital position. Thus, it is able to calculate more accurate pseudo-ranges and receiver location compared to batch processing and ways where statistical signal processing algorithms such as Kalman filter are performed directly on RINEX pseudo-ranges. It is also understood that by averaging the pseudo-ranges or any other parameters such as TEC obtained from RINEX data for 30 seconds assuming that all the visible satellites are looking at a same position on the earth. This analysis could give a good result when applied on each epoch as all the visible satellites at that epoch are looking at a same position on earth. It is also understood that by applying the satirical signal processing algorithms for every epoch leads to a more precise uncertain GPS positioning which can be used as initialization parameters for the applications mentioned above. The methodology if implemented on both L1 and L2 signals will give enhanced precise positioning using GPS.

References

[1] Nicholls, R. J., Hanson, S. E., Lowe, J. A., Slangen, A. B., Wahl, T., Hinkel, J., & Long, A. J. (2021). Integrating new sea-level scenarios into coastal risk and adaptation assessments: An ongoing process. Wiley Interdisciplinary Reviews: Climate Change, 12(3), e706.

[2] Allison, L. C., Palmer, M. D., & Haigh, I. D. (2022). Projections of 21st century sea level rise for the coast of South Africa. Environmental Research Communications, 4(2), 025001.

[3] Kint, L., Hademenos, V., De Mol, R., Stafleu, J., van Heteren, S., & Van Lancker, V. (2021). Uncertainty assessment applied to marine subsurface datasets. Quarterly Journal of Engineering Geology and Hydrogeology, 54(1).

[4] McCammon, S., Marcon dos Santos, G., Frantz, M., Welch, T. P., Best, G., Shearman, R. K., ... & Hollinger, G. A. (2021). Ocean front detection and tracking using a team of heterogeneous marine vehicles. Journal of Field Robotics, 38(6), 854-881.

[5] Borrelli, M., Smith, T. L., & Mague, S. T. (2021). Vessel-Based, Shallow Water Mapping with a Phase-Measuring Sidescan Sonar. Estuaries and Coasts, 1-19.

[6] Guariglia, A., Buonamassa, A., Losurdo, A., Saladino, R., Trivigno, M. L., Zaccagnino, A., & Colangelo, A. (2006). A multisource approach for coastline mapping and identification of shoreline changes.

[7] Gonçalves, R., Awange, J., & Krueger, C. (2013). GNSS-based monitoring and mapping of

shoreline position in support of planning and management of Matinhos/PR (Brazil). Journal of Global Positioning Systems, 11, 156-168.

[8] Kaliraj, S., Chandrasekar, N., & Ramachandran, K. K. (2017). Mapping of coastal landforms and volumetric change analysis in the south west coast of Kanyakumari, South India using remote sensing and GIS techniques. The Egyptian Journal of Remote Sensing and Space Science, 20(2), 265-282.

[9] Pereira, R. L., Trindade, J., Gonçalves, F., Suresh, L., Barbosa, D., & Vazão, T. (2013). A wireless sensor network for monitoring volcanic tremors.

[10] Revathi, R., Ramesh, K. S., Koteswara Rao, S., & Uday Kiran, K. (2018). Application of Parametric Methods for Earthquake Precursors Using GPS TEC. In Information and Decision Sciences (pp. 305-314). Springer, Singapore.

[11] Blewitt, G., Hammond, W. C., Kreemer, C., Plag, H. P., Stein, S., & Okal, E. (2009). GPS for real-time earthquake source determination and tsunami warning systems. Journal of Geodesy, 83(3), 335-343.

[12] Larson, K. M., Löfgren, J. S., & Haas, R. (2013). Coastal sea level measurements using a single geodetic GPS receiver. Advances in Space Research, 51(8), 1301-1310.

[13] Januszewski, J. (2014). Nominal and Real Accuracy of the GPS Position Indicated by Different Maritime Receivers in Different Modes. TransNav: International Journal on Marine Navigation and Safety of Sea Transportation, 8(1).

[14] Uddin, M. P., Islam, M. Z., Nadim, M., & Afjal, M. I. (2013). GPS-based location tracking system via Android device. Int. J. Res. Comput. Eng. Electron, 2(5).

[15] Kadibagil, M., & Guruprasad, H. S. (2014). Position detection and tracking system. International Journal of Computer Science and Information Technology & Security (IJCSITS), 4(3), 67-73.

[16] Genrich, J. F., & Bock, Y. (1992). Rapid resolution of crustal motion at short ranges with the Global Positioning System. Journal of Geophysical Research: Solid Earth, 97(B3), 3261-3269.

[17] Genrich, J. F., Bock, Y., & Mason, R. G. (1997). Crustal deformation across the Imperial fault: Results from kinematic GPS surveys and trilateration of a densely spaced, small-aperture network. Journal of Geophysical Research: Solid Earth, 102(B3), 4985-5004.

[18] Souza, E. M. D., Monico, J. F. G., & Pagamisse, A. (2009). GPS satellite kinematic relative positioning: analyzing and improving the functional mathematical model using wavelets. Mathematical Problems in Engineering, 2009.

[19] Revathi, R., Ramesh, K. S., Koteswara Rao, S., & Kiran, K. U. (2018). Application of Least Squares Algorithm for Precise GPS Receiver Positioning. In Information and Decision Sciences (pp. 297-303). Springer, Singapore.

[20] Revathi, R., Ramesh, K. S., Koteswara Rao, S., & Uday Kiran, K. (2018). Instantaneous time smoothing in GPS receivers using kalman filter. In Information and Decision Sciences (pp. 289-296). Springer, Singapore.

[21] Strang, G. (2020). Linear algebra for everyone. Wellesley-Cambridge Press.

[22] Tsui, J. B. Y. (2005). Fundamentals of global positioning system receivers: a software approach (Vol. 173). John Wiley & Sons.

[23] Murthy, A. S. D., Syamala, T., Rao, S. K., & Das, R. P. Real Time Differential Global Positioning System Using Fuzzy Logic Extended Kalman Filter. Journal of Advanced Research in Dynamical and Control Systems, 9.

[24] Sunehra, D. (2013). Validation of GPS receiver instrumental bias results for precise navigation. 92.60. Ls; 84.40. Ua; 91.10. Fc.

[25] Zhang, X., Landis, J. B., Sun, Y., Zhang, H., Feng, T., Lin, N., ... & Sun, H. (2021). Insights into the drivers of radiating diversification in biodiversity hotspots using Saussurea (Asteraceae) as a case. bioRxiv.

[26] Cardinal, T., Audin, L., Rolland, Y., Schwartz, S., Petit, C., Zerathe, S., ... & Guillou, V. (2021). Interplay of fluvial incision and rockfalls in shaping periglacial mountain gorges. Geomorphology, 381, 107665.

[27] Chardon, V., Schmitt, L., Arnaud, F., Piégay, H., & Clutier, A. (2021). Efficiency and sustainability of gravel augmentation to restore large regulated rivers: Insights from three experiments on the Rhine River (France/Germany). Geomorphology, 380, 107639.

[28] Astudillo-Sotomayor, L., Jara-Muñoz, J., Melnick, D., Cortés-Aranda, J., Tassara, A., & Strecker, M. R. (2021). Fast Holocene slip and localized strain along the Liquiñe-Ofqui strike-slip fault system, Chile. Scientific reports, 11(1), 1-10.

[29] Mr. Kaustubh Patil. (2013). Optimization of Classified Satellite Images using DWT and Fuzzy Logic. International Journal of New Practices in Management and Engineering, 2(02), 08 - 12. Retrieved from http://ijnpme.org/index.php/IJNPME/article/view/15

[30] Viveen, W., Sanjurjo-Sanchez, J., Baby, P., & del Rosario González-Moradas, M. (2021). An assessment of competing factors for fluvial incision: An example of the late Quaternary exorheic Moyobamba basin, Peruvian Subandes. Global and Planetary Change, 200, 103476.

[31] Sai, M. P., Amaleswara Rao, V., Suvarna Vani, K., & Poul, P. (2022). Prediction of housing price and forest cover using mosaics with uncertain satellite imagery. International Journal on Recent and Innovation Trends in Computing and Communication, 10(8), 36-46. doi:10.17762/IJRITCC.V10I8.5666

[32] Jat, N. C., & Kumar, C. (2022). Design assessment and simulation of PCA based image difference detection and segmentation for satellite images using machine learning. International Journal on Recent and Innovation Trends in Computing and Communication, 10(3), 1-11. doi:10.17762/ijritcc.v10i3.5520

[33] Nalivan, O. A., Badehian, Z., Sadeghinia, M., Soltani, A., Islami, I., & Boustan, A. (2022). A step beyond susceptibility: an adaptation of risk framework for monetary risk estimation of gully erosion. Natural Hazards, 1-24.